RSC Advances

ROYAL SOCIETY OF CHEMISTRY

www.rsc.org/advances

Property of YAG:Ce^{3+} nanophosphors prepared by solvothermal method using triethylene-tetramine as reaction solvent

Likai Wang[1], Fenghua Zhao[1*], Xianfeng Yang[2], Chunyang Pan[1], Huimin Huang[1]

[1]School of Light Industry and Chemical Engineering, Guangdong University of Technology, Guangzhou 510006, China.

[2]Analytical and Testing Center, South China University of Technology, Guangzhou, 510641, China.

E-mail address: [1] wlk525.lcu@163.com [2] Xianfeng78@hotmail.com

*Corresponding author

School of Light Industry and Chemical Engineering, Guangdong University of Technology, Guangzhou 510006, China.

Email address: seazhaofh@163.com TEL: +86 13560183936

Abstract

In this study, spherical YAG:Ce^{3+} nanophosphors (NPs) with a particle size of 200 nm were successfully synthesized by a solvothermal method using triethylene-tetramine (TETA) as reaction solvent. Besides as the reaction medium, TETA also acted as the precipitant for the formation of hydroxide precursors at the initial stage of the solvothermal reaction. The shape of the particle prepared with 4 mL of TETA as precipitant is more regular spherical and larger size (about 500 nm). The phase compositions, microstructures and photoluminescent properties of the as-prepared YAG:Ce^{3+} NPs were investigated via X-ray powder diffraction (XRD), fourier transform infrared spectroscopy (FTIR), scanning electron microscopy (SEM), transmission electron microscopy (TEM) and fluorescence spectrophotometer. To improve PL properties of as-prepared YAG:Ce^{3+} NPs, the holding time, Ce^{3+} doping concentration and filling factor of autoclave have been systematically optimized. The optimal cerium doping concentration is 3 mol%.

Key words:

Solvothermal method; YAG:Ce^{3+} nanophosphors; Photoluminescent properties; Triethylene-tetramine

1. Introduction

Trivalent cerium-doped yttrium aluminum garnet ($Y_3Al_5O_{12}$), abbreviated as YAG:Ce^{3+}, is a studied earliest and most completely yellow phosphor. YAG:Ce^{3+} phosphors can convert a blue light from an InGaN-based light-emitting diode (LED) into a very broad yellow emission, generating a white light by the combination of the residual blue light and the yellow emission. Due to this optical function, YAG:Ce^{3+} phosphors have been widely applied in solid-state lightings and display systems [1-3].

An extremely high temperature near 1600 ^{o}C is required for the conventional synthesis of phase pure YAG through a traditional solid-state method using Y_2O_3 and Al_2O_3 as starting materials [4,5]. Due to the high temperature during the solid-state reaction, the aggregation of resultants can hardly be avoided and it would result in non-uniformity and large particle sizes (micrometer or submicrometer). Since the Rayleigh scattering intensity of a particle is proportional to the sixth power of the particle diameter, smaller particle possesses a higher surface to volume ratio, which would increase the efficiency of absorption and emission. Therefore, nano-sized phosphors may contribute to reduce the optical scattering loss [6]. To prepare YAG:Ce^{3+} phosphor with a small particle size and high quality, several wet soft-chemical synthetic techniques including co-precipitation [7], spray-drying [8-10] and sol-gel methods [3,11] have been developed in recent years. However, co-precipitation method and sol-gel method as well as the solid-state reaction may lead to the oxidation of Ce^{3+} into Ce^{4+} and the formation of impurity phases during the post thermal treatments [12].

With the development of the above wet soft-chemical methods, some researchers reported that the hydrothermal method under the critical point of the water (T_s =374 ^{o}C, P_s = 22.4 MPa) can be used to prepare the pure YAG and rare earth-doped YAG nanoparticles with narrow grain size distribution and

high dispersibility [13-15]. Solvothermal method enable us to prepare the crystalline YAG close to 300 ^{o}C and appears more suitable for the synthesis of the nanoparticles compared with hydrothermal method [16-18]. 1,4-butylene glycol was used as the solvent in the solvothermal method at 300 ^{o}C to prepare the phase pure YAG by Inoue et al, which was called as the glycothermal method [16]. Similarly, Isobe and coworkers reported that YAG:Ce^{3+} nanocrystals of 10 nm diameter can be prepared by the glycothermal method [17]. In addition, they revealed the effect of surface modification on the PL enhancement of YAG:Ce^{3+} nanocrystals. Motivated by Isobe' s work, Nyman et al [18] adopted the same synthetic route with some modifications to prepare YAG:Ce^{3+} nanocrystals, where the reaction temperature was 225 ^{o}C and reaction time was 4-14 days. Jia et al [1] prepared well dispersed spherical YAG:Ce^{3+} phosphors by the solvothermal method where nitrate of yttrium, cerium and aluminium were dissolved and mixed in the autoclave induced with ethylenediamine as the solvent at 210 ^{o}C for 15 h. According to the above reports, it is obvious that the organic reaction medium has played an important role in the formation and optical properties of YAG:Ce^{3+} NPs during the solvothermal process.

As reported in our previous works [19], triethylene-tetramine (TETA) has been already used as a precipitant to form the hydroxide precursors. In this paper, TETA solvent was employed as a reaction medium in the solvothermal process to prepare YAG:Ce^{3+} nanophosphors (NPs) for the first time. The purpose of this work was to investigate the influence of the dosage of TETA, holding time, Ce^{3+} doping concentration and filling factor of autoclave on the as-prepared YAG:Ce^{3+} NPs properties to optimize. the synthetic solvothermal conditions guiding the most efficient YAG:Ce^{3+} NPs.

2. Experiments

Yttrium nitrate hexahydrate ($Y(NO_3)_3 \cdot 6H_2O$, 99.5%), aluminum nitrate nonahydrate ($Al(NO_3)_3 \cdot 9H_2O$, 99%), cerium nitrate hexahydrate ($Ce(NO_3)_3 \cdot 6H_2O$, 99%), triethylene-tetramine (TETA, 95%) and absolute ethanol were used as received without further purification. Aqueous solutions were prepared using distilled

water.

The mother salt solution was prepared by dissolving a multi-cation aqueous solution. $Y(NO_3)_3 \cdot 6H_2O$, $Al(NO_3)_3 \cdot 9H_2O$ and $Ce(NO_3)_3 \cdot 6H_2O$ into 15 mL of absolute ethanol according to stoichiometric proportions of $Y_{3-x}Al_5O_{12}:Ce_x$. The x was varied from 0.06 to 0.18, corresponding to 2 to 6 mol% of Ce^{3+} relative to (Y^{3+} + Ce^{3+}). The concentration of Y^{3+} ions was 0.1 mol/L. After through mixing for 30 min at room temperature, a certain amount of TETA was added into the above solution under magnetic stirring. The precursor solution was formed after continue stirring for 8 hours at ambient temperature. Then the precursor solution was filtered and washed with absolute ethanol for three times. The collected white precipitate was diluted in 10 mL of TETA and transferred into an autoclave with a capacity of 40 mL. The autoclave was sealed and then heated at 250 ^oC, and the holding time varied from 4 h to 120 h. After cooling to room temperature naturally, the products in the autoclave were washed with ethanol for three times and dried for 24 h at 80 ^oC for further study.

The phase and structure of the phosphors were characterized by powder X-ray diffractometer (XRD, Rigaku, D/max 2200) using Cu Kα radiation. Fourier transform infrared (FT-IR) absorption spectra were recorded on a spectrometer (Thermo-Nicolet 380) by means of a KBr disk method. Thermal gravimetric analysis and differential scanning calorimetry analysis (TG-DSC) of the sample were made on a TG-DSC analyzer (model STA-409-PC, NETZSCH, Germany). The sample was heated in air between 30 and 900 ^oC at a rate of 10 ^oC/min. The particle morphology and size were studied by scanning electron microscopy (SEM-S3400N, HITACHI), and all samples were coated with a thin layer of gold for conductivity before observation. The transmission electron microscopy (TEM) and high resolution transmission electron microscopy (HRTEM) work were done under a JEM-2010HR transmission electron microscope operated at an accelerating voltage of 200 kV. Photoluminescence property was measured with a fluorescence spectrophotometer (FluoroMax-4-VPF-100, HORIBA JOBIN JVON) equipped with a Xenon lamp. All the

measurements were carried out at room temperature.

3. Results and discussion

3.1 Effect of holding time on synthetic reaction and optical properties of YAG:Ce^{3+} NPs

Fig. 1 shows XRD patterns of YAG: Ce^{3+} phosphor powder synthesized at 250 ^{o}C for different holding times. The main diffraction peaks at 2θ = 18.1^{o}, 27.6 ^{o}, 29.7 ^{o}, 33.3 ^{o}, 36.4 ^{o}, 41.0 ^{o}, 46.6 ^{o}, 55.1 ^{o} and 57.4 ^{o} are corresponding to the cubic phase YAG (JCPDS card No. 33-0040) with the addition of Ce^{3+}. Though YAG phase was formed when the holding time was 4 h, the intensities of the diffraction peaks were low. The diffraction peak intensity was increased and the full-width at half maximum (FWHM) was decreased with the prolongation of holding time, which might be attributed to the gradual increase in the substituted Ce^{3+} content and the growth of particles with single crystallites [20,21]. Moreover, no cerium oxide or other intermediate oxide phases were observed, indicating that cerium is homogeneously dispersed at the atomic level in the YAG lattice via this synthetic approach [2].

Fig. 2 shows FT-IR spectra of YAG:Ce^{3+} NPs obtained with different holding time. The band near 3450 cm^{-1} was due to the stretching vibrations of N-H and O-H bands. The band at about 1630 cm^{-1} is a result from the bending vibration of H_2O [22]. The peak at 1380 cm^{-1} is corresponding to the asymmetric and symmetric stretching vibration and bending vibration of the C-H bond [23]. which suggest the presence of organic residual groups at the surface of particles. Besides, the intensity of absorption bands for various organic groups decreases and gradually pyrolyzes with the prolongation of holding time. The peaks at 790, 735, 615, 525 cm^{-1} can be assigned to metal-oxygen (M-O) vibrations of YAG structure, and the rise in intensity indicates the improvement of crystallinity with increasing the holding time as previously shown in XRD patterns [24].

The endothermic peak at about 492 ^{o}C and the exothermic peak at about 322 ^{o}C were observed in the DSC profile of sample (Fig. 3). The exothermic peak at about 322 ^{o}C was possibly assigned to the pyrolysis

of TETA adsorbed on the surface of as-prepared YAG:Ce^{3+} NPs. The endothermic peak at about 492 ^{o}C might be attributed to the structural change with the loss of weight, as referred to the thermal behavior of the alkyl derivatives of boehmite [25]. The TG profile shows the weight loss of sample which was accompanied with the endothermic or exothermic reaction shown in the DSC profile. The total weight loss of the sample was about 8 wt % below 900 ^{o}C.

The morphologies and structures of the samples have been investigated by SEM. The SEM images of samples obtained with different holding times are depicted by Fig. 4(a, b, c, d, e). The sample prepared for 4 h at 250 ^{o}C exhibited spherical shape and aggregate particle with a mean diameter of about 150-350 nm. For $t_h > 4$ h, the attraction force between them will increase with the growth of YAG particles. Therefore, aggregate size increased due to the Ostwald ripening process which forms larger particles at the expense of smaller ones [2]. When the holding time was 24 h, the particle size was about 200-350 nm. As the holding time is 72 h, the particle size is in a range between 250 nm and 450 nm. While the holding time was above 96 h, the particle shape is regular spherical and the range of particle size is 300-700 nm. which will cause the aggregation among the particles. The distribution of particle diameter became narrow and the shape of particle was more regular spherical with the prolongation of the holding time. The TEM images of sample prepared with 120 h of holding at 250 ^{o}C are depicted in Fig. 4(f, g), which show the particle size of the sample are consistent with Fig. 4(e). The selected area electron diffraction (SAED) pattern is shown in Fig. 4(h), indicating that the individual YAG:Ce^{3+} nanocrystals shows a single crystalline character. The HR-TEM image of a single nanocrystal is illustrated in Fig. 4(i). The HR-TEM image includes a series of crystal facets. The crystal lattice fringes with the spacing d values of 0.494 nm is observed, which corresponds to the (211) crystal facets of the cubic phase YAG (JCPDS card No. 33-0040).

Generally, the factors including sizes, morphologies, crystallinities and number of defects have a profound effect on the PL properties of samples. As shown by Fig.5, the PL emission intensity of samples increases

with the prolongation of holding time, which might be attributed to the gradual increase in the substituted Ce^{3+} content and the growth of particles with single crystalline. There are the ground $4f^1$ and the excited $4f^05d^1$ state in the electronic transition of Ce^{3+}. The emission spectra is assigned to the $5d(^2A_{1g})\rightarrow 4f(^2F_{5/2}$ and $^2F_{7/2})$ transitions of Ce^{3+}, since Ce^{3+} with a $4f^1$ electron configuration has two ground states of $^2F_{5/2}$ and $^2F_{7/2}$ due to the spin-orbit coupling [17]. The PL emission spectra of samples obtained with 4 h and 24 h of holding are blue shifted compared to those obtained with 72-120 h of holding time. It is well known that the 5d-4f emission of Ce^{3+} depends on the crystal field. The smaller particles obtained with 4 h and 24 h have a higher surface tension than that of larger ones obtained with 72-120 h, hence the 5d level would have a stronger crystal-field splitting [24,26]. Meanwhile, the shift could also be attributed to the enhancement of crystallinity and the decrease in Ce^{3+}/Ce^{4+} ratio with the prolongation of holding time [2].

3.2 Effect of filling factor on morphologies and PL properties of YAG:Ce^{3+} NPs

In this study, the effect of filling factor of the autoclave on grain morphologies of YAG:Ce^{3+} nanophosphor powders were also investigated. The morphologies of YAG:Ce^{3+} nanophosphor powders with the variation of filling factor of the autoclave are shown in Fig. 6(a, b, c, d). Firstly, the particle shape of sample is regular spherical and the particle size reaches about 400- 600 nm when the filling factor is below 50 %. However, increasing the filling factor above 50 %, the particle shape becomes irregular and the size distribution is wide due to the pressure of reaction system rising, the speed of the mass transfer, grain growth and grain crystallinity increasing [1]. The selected area electron diffraction (SAED) patterns is illustrated in Fig. 6(e), indicating that the individual YAG: Ce^{3+} nanocrystals shows a single crystalline character. The HR-TEM image of a single nanocrystal is illustrated in Fig. 6(f). The HR-TEM image includes a series of crystal facets.the crystal lattice fringes with the spacing d values of 0.494 and 0.306 nm are observed, which corresponds to the (211) and (400) crystal facets of the cubic phase YAG (JCPDS card No. 33-0040), respectively.

Besides, increasing the filling factor of reaction system leads to the rise of the pressure of reacting system, which can speed up the diffusion of rate of Ce^{3+}, grain growth and grain crystallinity, Therefore, the PL emission intensity of YAG: Ce^{3+} phosphors are enhanced. Meanwhile, the sample obtained with 25 % of filling factor is blue shifted by about 12 nm compared to that obtained with 75 % of filling factor due to the enhancement of crystallinity as shown in Fig. 7.

3.3 Effect of dosage of triethylene-tetramine on morphologies of YAG:Ce^{3+} NPs

As reported in our previous work [19], pH of the precursor solution changes with the variation of dosage of TETA in the process of precipitation. Since the pH of the precursor solution affect the precipitated ratio of Y^{3+} and Al^{3+} [7], then the dosage of TETA is the critical factor which strongly influences the morphological and photoluminescent properties of YAG: Ce^{3+} phosphor. As shown by the SEM investigation in Fig. 8(a, b, c), the particle of sample consists of spherical and irregular fragment when the volume of TETA is 0.5 mL. Increasing to 2 mL of TETA, YAG:Ce^{3+} powder is homogeneous, being composed of spherical particles with an average size ranging from 200 nm to 300 nm. Furthermore, the shape of the particle prepared with 4 mL of TETA is more regular spherical and larger size (about 500 nm) compared to that of particle prepared with 2 mL of TETA. The emission intensity increased monotonically with the increase of the volume of TETA from 0.5 mL to 4.0 mL as illustrated in Fig. 9. Due to hydroxides of Al^{3+} and Y^{3+} appearing at a pH of 3.5 and 8.1 separately, the heterogeneous distribution of Al^{3+} and Y^{3+} will occur when the pH value is less than 8.1, resulting in the ratio of Y^{3+} and Al^{3+} deviating from 3:5 in local areas [19].

3.4 Effect of Ce^{3+} concentration on PL properties of YAG:Ce^{3+} NPs

The effect of varying Ce^{3+} concentrations on optical properties of $Y_{3-x}Al_5O_{12}:Ce_x$ phosphors were also investigated. As shown in Fig.10, the emission intensity increased monotonically with the increase in Ce^{3+} concentration up to x=0.09 ($Y_{3-x}Al_5O_{12}:Ce_x$, x=0.06-0.18). However, the emission intensity decreased

beyond the limit value due to the effect of concentration quenching[27-30]. As excessive Ce^{3+} ions are doped into the host, the distance of Ce^{3+}-Ce^{3+} will reduce. Then the energy transfer occurs between Ce^{3+} ions which affects the immigration of excitation energy, leading to the decrease of emission intensity [31,32]. The red shift of emission occurred from 526 to 536 nm with the variation of x varying from 0.06 to 0.18, which can be explained by magnetic interactions between neighboring Ce^{3+} ions [24].

4. Conclusions

In this work, Ce-doped YAG ultra-fine particles were successfully synthesized by the solvothermal method, which were induced in an autoclave where TETA solution was firstly used as solvent at 250 ^{o}C for 4 h. For t_h >4 h，the average size of particles increases to reach about 500 nm and the particle shape is more regular spherical for 120 h of holding time. With the prolongation of holding time and increase in filling factor, the PL emission intensity of YAG:Ce^{3+} phosphors increase due to the gradual increase in the substituted Ce^{3+} content and the growth of particles with single crystalline. The most efficient YAG:Ce NPs can be prepared with 4 mL of TETA as a precipitator at 250 ^{o}C for 120 h and 3 mol% of Ce^{3+} with 75% of filling factor. This synthesis process was relatively simple and could be easily controlled, which is suitable for applications requiring a high degree of homogeneity such as optical devices and provides a better control of the final product at the molecular level. This synthetic method holds good potential application in solid-state lighting.

Acknowledgements

This work was supported by the National Natural Science Foundation of China (51002034) and China Postdoctoral Science Foundation (2012M521572) and Technology Rising Star of Guangzhou Foundation (2012J2200099) and the Technology Program of Guangdong Province (2013B090500050).

References:

[1] N.T. Jia, X.D. Zhang, W. He, W.J. Hu, X.P. Meng, Y. Du,J.C. Jiang, Y.W. Du, J. Alloys Comp., 2011, 509, 1848.

209 [2] A. Aboulaich, J. Deschamps, R. Deloncle, A. Potdevin, B. Devouard, G. Chadeyron, R. Mahiou, New. J.
210 Chem., 2012, 36, 2493.
211 [3] Y.X. Pan, M.M. Wu, Q. Su, Mater. Sci. Eng. B., 2004, 106, 251.
212 [4] A. Ikesue, I. Furusato, J. Am. Ceram. Soc., 1995, 78, 225.
213 [5] Z. Song, J. Liao, X.L. Ding, X.L. Liu, Q.L. Liu, J. Cryst.Growth., 2013, 365, 24.
214 [6] H.J. Byun, W.S. Song, Y.S. Kim, H. Yang, J. Phys. D: Appl. Phys., 2010, 43, 1.
215 [7] H.Z. Wang, L. Gao, K. Niihara, Mater. Sci. Eng., A. 2000, 288, 1.
216 [8] J. S. Cho and Y. C. Kang, RSC Adv., 2014, 4, 25234.
217 [9] J. S. Cho, S. M. Lee, K. Y. Jung and Y. C. Kang, RSC Adv., 2014, 4, 43606.
218 [10] J. S. Cho, K. Y. Jung, and Y. C. Kang, RSC Adv., 2015, 5, 8345.
219 [11] M. Veith, S. Mathur, A. Kareiva, M Jilavi, M. Zimmer, V. Huch, J. Mater. Chem., 1999, 9, 3069.
220 [12] R.J. Ji, W.H. Yin, C.X. Fang, and Y.W. Zeng, J. Mater. Chem. C., 2013, 1, 1763.
221 [13] Q.X. Zheng, B. Li, H.D. Zhang, J.J. Zheng, M.H. Jiang, X.T. Tao. J. Supercrit. Fluids., 2009, 50, 77.
222 [14] Y. Hakuta, K. Seino, H. Ura, T. Adschiri, H. Takizawa,K. Arai, J. Mater. Chem., 1999, 9, 2671.
223 [15] Y. Hakuta, T. Haganuma, K. Sue,T. Adschiri, K. Arai, Mater. Res. Bull., 2003, 38, 1257.
224 [16] M. Inoue, H. Kominami, T. Inui, J. Am. Ceram. Soc., 1990, 73, 1100.
225 [17] R. Kasuya, T. Isobe, H. Kuma, J. Alloys Comp., 2006, 408–412, 820.
226 [18] M. Nyman, L.E. Shea-Rohwer, J. E. Martin, P. Provencio, Chem. Mater., 2009, 21, 1536.
227 [19] L. K. Wang, F. H. Zhao, J. L. Zhuang, C. Y. Pan, H. M. Huang, Mater. Lett., 2014, 120, 163.
228 [20] Z.G. Wu, X.D. Zhang, W. He, Y.W. Du, N.T. Jia, G.G. Xu, J. Alloys Comp., 2009, 468, 571.
229 [21] G.Q. Chai, G.P. Dong, J.R. Qiu, Q.Y. Zhang, Z.M. Yang, J. Phys. Chem. C., 2012, 116, 19941.
230 [22] K. Zhang, H.Z. Liu, Y.T.Wu, W.B. Hu, J. Alloys Comp., 2008, 453, 265.
231 [23] S.P. Kuang, Z.Z. Wang, J. Liu, Z.C. Wu, J. Hazard. Mater., 2013, 260, 210.

[24] K. Zhang, H.Z. Liu, Y.T. Wu, W.B. Hu, J. Mater. Sci., 2007, 42, 9200.

[25] M. Inoue, M. Kimura, Mol. Cryst. Liq. Cryst., 2000, 341, 431.

[26] Q. Li, L. Gao, D.S. Yan, Mater. Chem. Phys., 2000, 64, 41.

[27] S. Som, A.K. Kunti, V. Kumar, V. Kumar, S. Dutta, M. Chowdhury, S.K. Sharma, J.J. Terblans, H.C. Swart, J. Appl. Phys. ,2014, 115, 193101.

[28] S. Som, P. Mitra, V. Kumar,V. Kumar, J. J. Terblans, H. C. Swart, S. K. Sharma, Dalton Trans., 2014, 43, 9860.

[29] V. Kumar, S. Som, V. Kumar, V. Kumar, O.M. Ntwaeaborwa, E. Coetsee, H.C. Swar, Chem Eng J., 2014, 255, 541.

[30] S. Som, S. Dutta, V. Kumar, A. Pandey, V. Kumar, A.K. Kunti, J. Priya, S.K. Sharma, J.J. Terblans, H.C. Swart, J. Alloys Comp., 2015, 622, 1068.

[31] P. Rai, M.K. Song, H.M. Song, J.H. Kim, Y.T. Yu. Ceram. Int., 2012, 38, 235.

[32] V.P. Dotsenko, I.V. Berezovskaya, E.V. Zubar, N.P. Efryushina, N.I. Poletaev, Yu.A. Doroshenko, G.B. Stryganyuk, A.S. Voloshinovskii, J. Alloys Comp., 2013, 550, 159.

List of figure captions:

Table 1. All experimental conditions.

Fig. 1 XRD patterns of YAG:Ce^{3+} NPs synthesized at 250 ^{o}C for different holding times.

Fig. 2 FT-IR spectra of precursors, YAG: Ce^{3+} NPs obtained with different holding times.

Fig. 3 TG-DSC profiles of sample prepared at 250 ^{o}C for 120 h.

Fig. 4 SEM images of samples prepared with different holding times at 250 ^{o}C: (a) 4 h, (b) 24 h, (c) 72 h, (d) 96 h, (e) 120 h. (f), (g) TEM images of sample prepared with 120 h of holding at 250 ^{o}C. (h) SAED pattern of sample synthesized by 120 h of holding at 250 ^{o}C. (i) HR-TEM image of the sample prepared with 120 h of holding at 250 ^{o}C.

Fig. 5 The PL emission spectra of YAG:Ce^{3+} NPs synthesized by different holding times at 250 ^{o}C.

Fig. 6 SEM images of YAG: Ce^{3+} NPs prepared with different filling factors: (a) 12.5 %, (b) 25 %, (c) 75 % and (d) 50 %. (e) SAED pattern of sample synthesized by 50 % of filling. (f) HR-TEM image of the sample prepared with 50 % of filling.

Fig. 7 The PL emission spectra of YAG:Ce^{3+} phosphors prepared with different filling factors.

Fig. 8 SEM images of YAG: Ce^{3+} NPs synthesized by different dosage of TETA as precipitato

r: (a) 0.5 mL, (b) 2 mL, (c) 4 mL.

Fig. 9 The PL emission spectra of YAG: Ce^{3+} NPs synthesized by different dosage of triethylene tetramine as precipitator: (a) 0.5 mL, (b) 2 mL, (c) 4 mL.

Fig. 10 The PL emission spectra of $Y_{3-x}Al_5O_{12}:Ce_x$ phosphors with various Ce^{3+} doping concentrations x in the range from 0.06 to 0.18**.**

Sample no.	X	Temperature/^{o}C	Holding time/h	Precipitator/mL	Solvent/mL	Filling factor/%
S1	0.06	250	120	4.0	10	25.0
S2	0.09	250	120	4.0	10	25.0
S3	0.14	250	120	4.0	10	25.0
S4	0.18	250	120	4.0	10	25.0
S5	0.14	250	96	4.0	10	25.0
S6	0.14	250	72	4.0	10	25.0
S7	0.14	250	24	4.0	10	25.0
S8	0.14	250	8	4.0	10	25.0
S9	0.14	250	4	4.0	10	25.0
S10	0.14	250	120	2.0	10	25.0
S11	0.14	250	120	0.5	10	25.0
S12	0.14	250	120	4.0	5	12.5
S13	0.14	250	120	4.0	20	50
S14	0.14	250	120	4.0	30	75

Table. 1

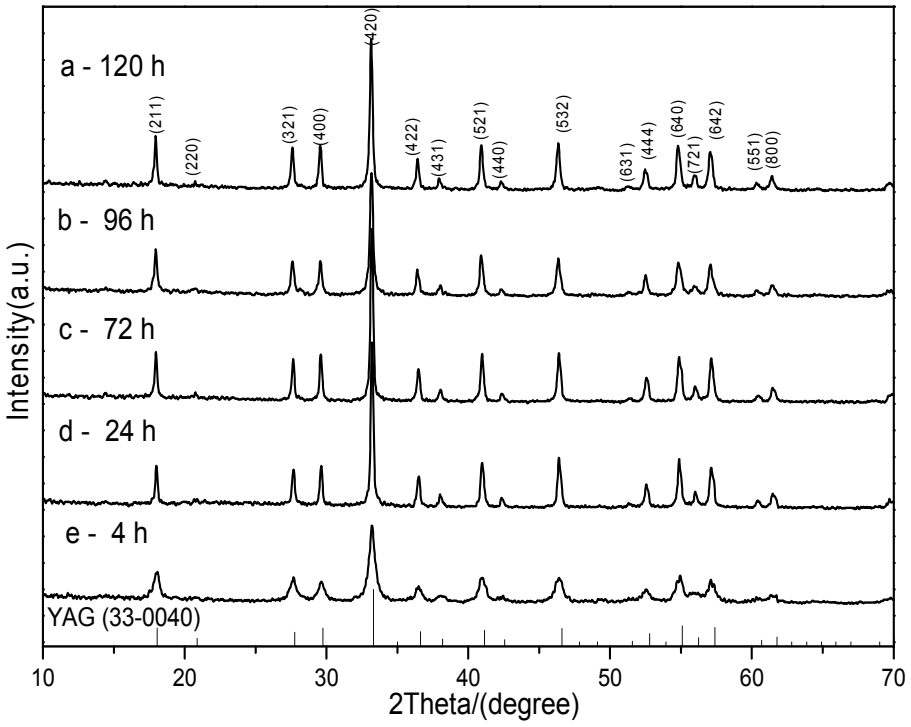

Fig. 1

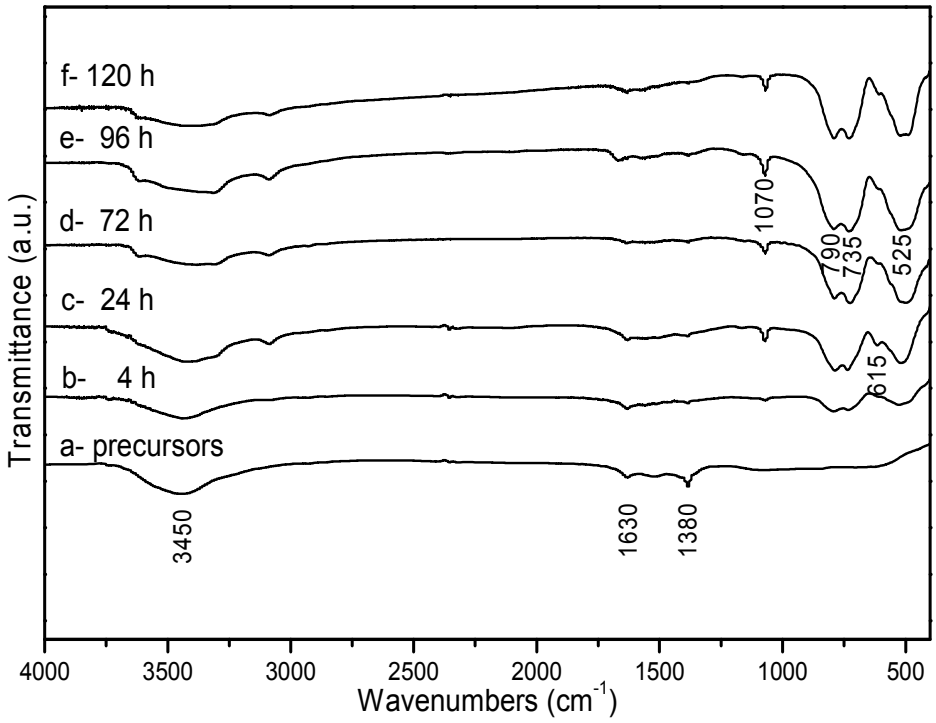

Fig. 2

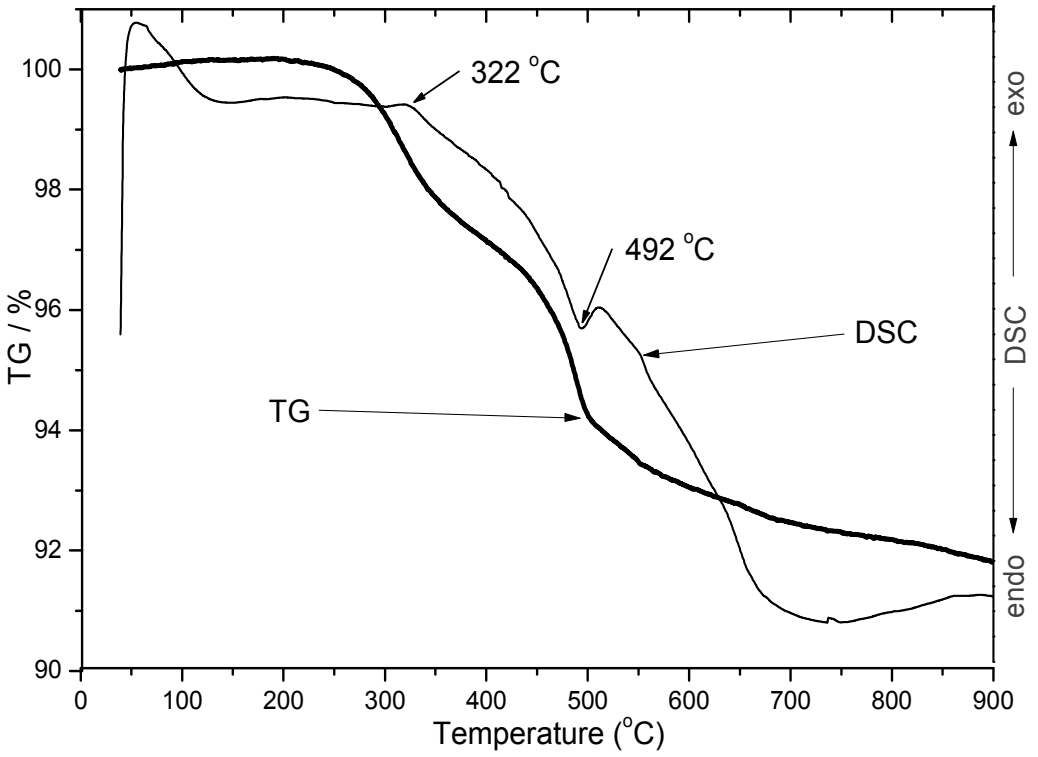

Fig. 3

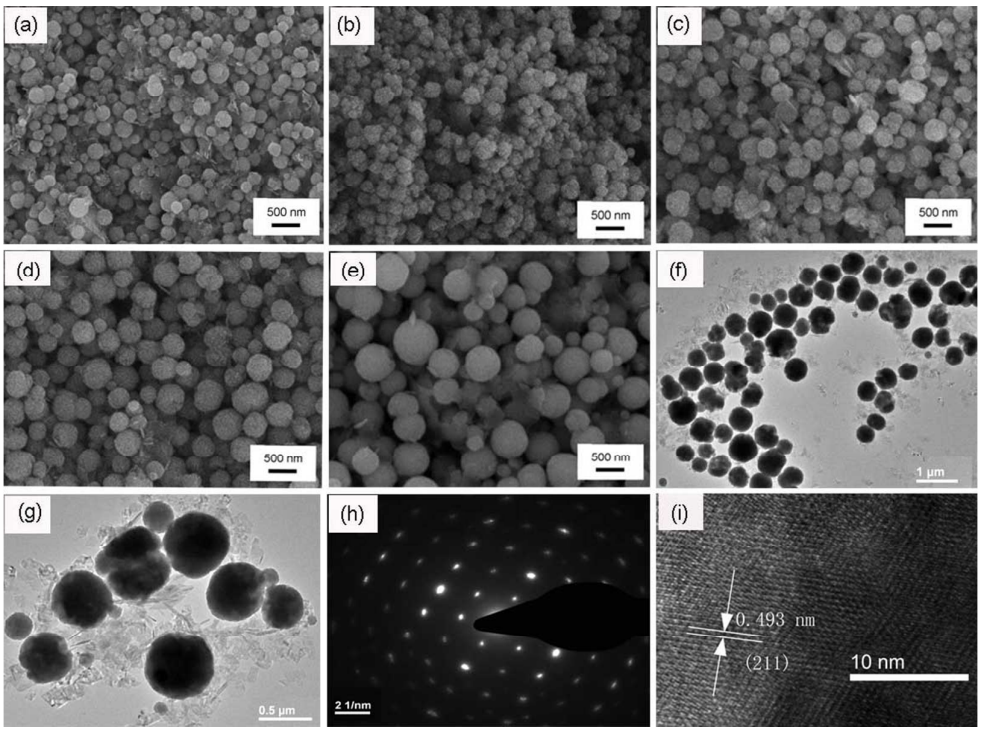

Fig. 4

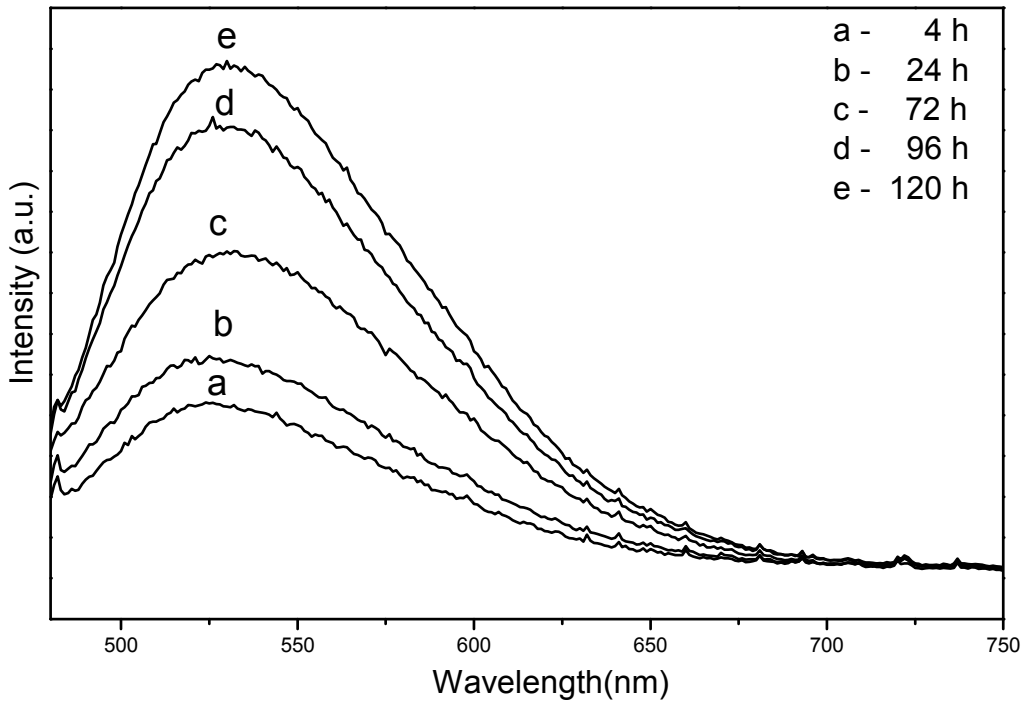

Fig. 5

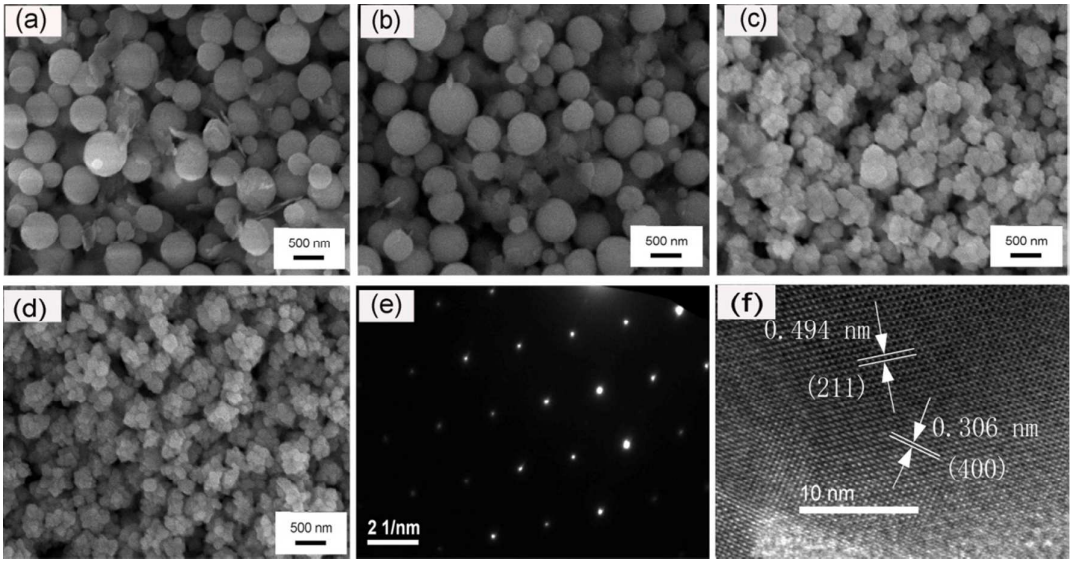

Fig. 6

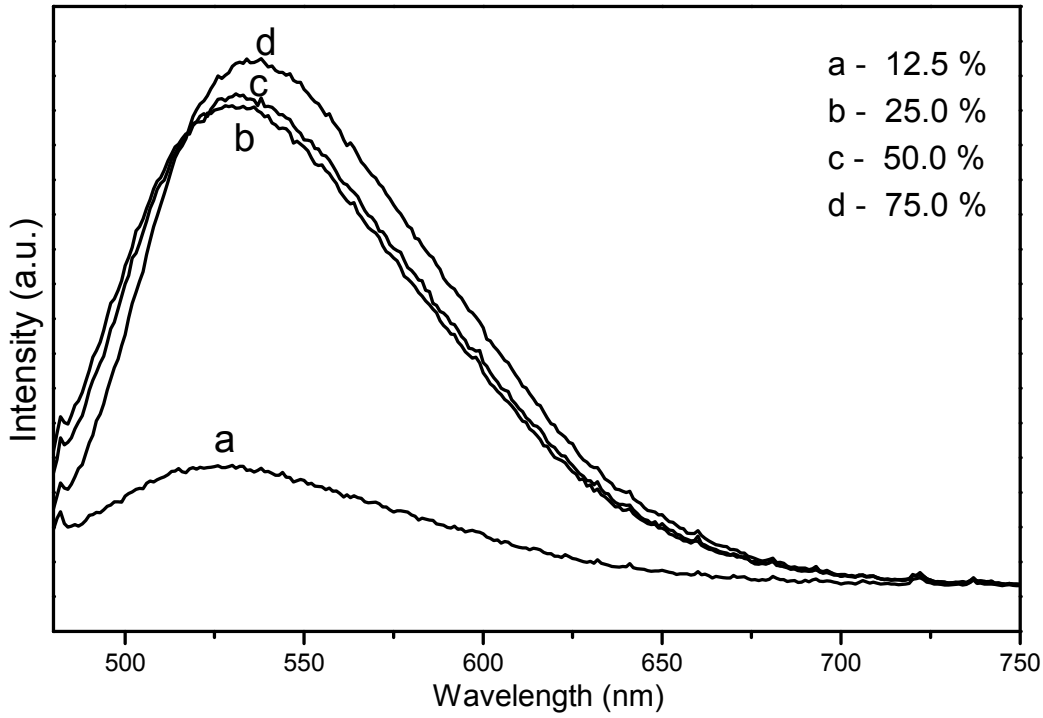

Fig. 7

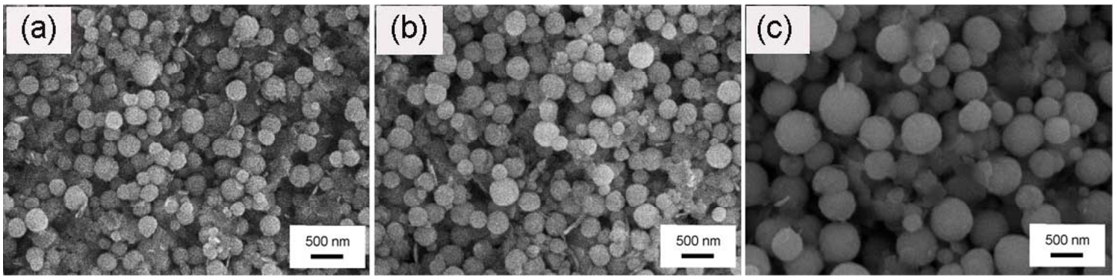

Fig. 8

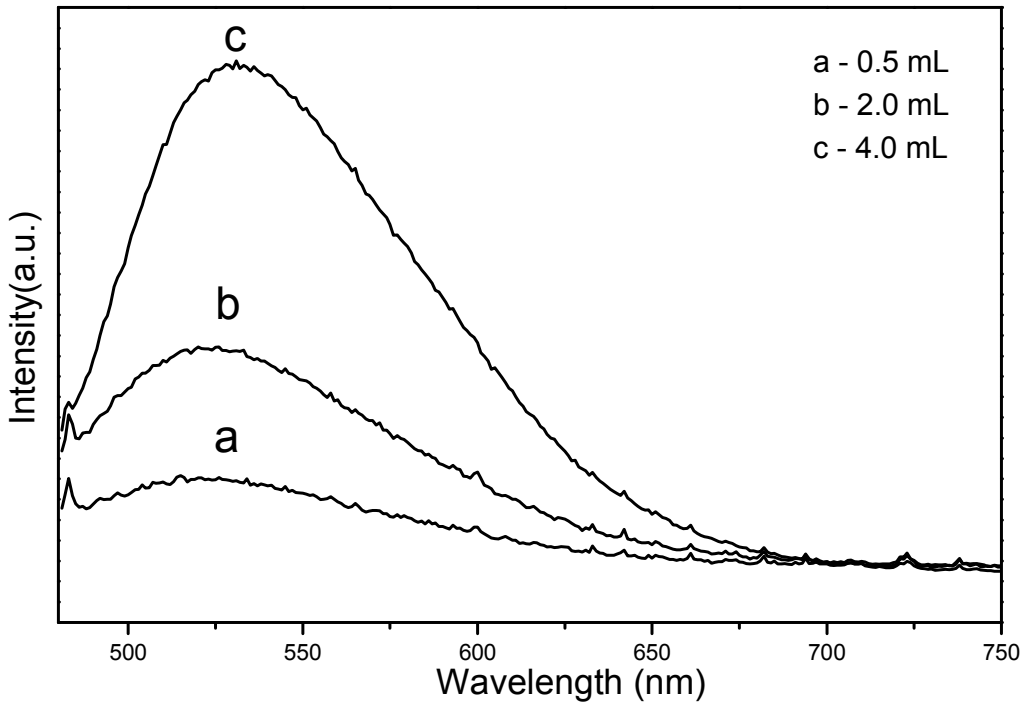

Fig. 9

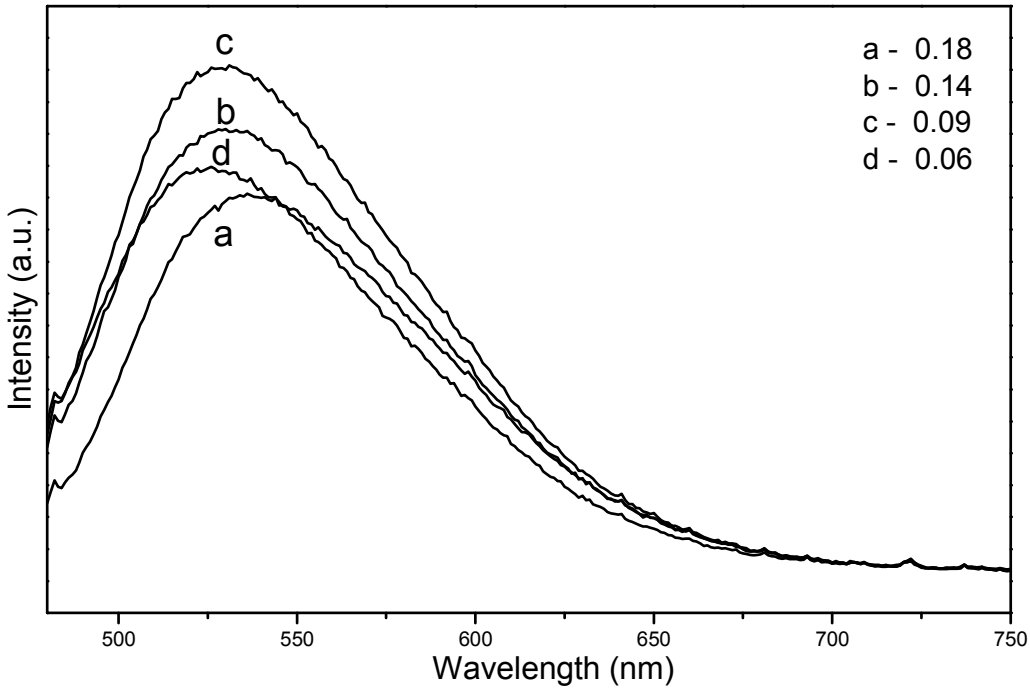

Fig. 10